DETECTION OF EARLY STAGE LARGE SCALE LANDSLIDES IN FORESTED AREAS BY 2 M LiDAR DEM ANALYSIS
THE EXAMPLE OF PORTAINÉ (CENTRAL PYRENEES)

Marta Guinau (1), Maria Ortuño (1), Jaume Calvet (1), Glòria Furdada (1), Jaume Bordonau (1), Antonio Ruiz (2) and Miquel Camafort (3)

(1) RISKNAT, GEOMODELS Research Institute, Dept. Geodinàmica i Geofísica, Facultat de Geologia, Universitat de Barcelona (UB), Martí i Franquès s/n, 08028 Barcelona, Spain (mguinau@ub.edu)
(2) Institut Cartogràfic i Geològic de Catalunya (ICGC), Parc de Montjuïc, 08038 Barcelona, Spain, (antonio.ruiz@icgc.cat)
(3) Institut de Ciències del Mar-CSIC, Psg. Marítim de la Barceloneta, 37-49, 08003 Barcelona, Spain, (camafort@icm.csic.es)

European Geosciences Union
General Assembly 2016
Vienna |Austria | 17 – 22 April 2016

1- Introduction

Lidar Digital Elevation Models (DEM) are useful to detect and measure subtle landforms generated in early stages of mass movements often undetectable by other methods. Lidar DEM

i) allows to detect small changes in slope

ii) permits to analyze the bare ground below the canopy in forested terrains

iii) furnishes an overview of the landforms within a wide area

The geomorphological study by using LiDAR data in a sector of the Pyrenees lacking of a regional landslide inventory map has revealed landforms associated to incipient deep-seated gravitational landslides and complex landslides. From this analysis, the failure mechanisms, the failure surface geometry in depth and the controlling and triggering factors such as lithology, geological structures, and stress changes due to glacial retreat or seismic amplification for a given source are discussed.

2- Study area: geological and geomorphological settings

The study area is located in the Central Pyrenees in an antiformal domain called the Orri dome formed during the Alpine orogeny (Mesozoic–Cenozoic times) (Poblet, 1991).

The bedrock of the Orri dome consists of Cambro-Ordovician metasedimentary materials (mm and cm-thick layers of slate strongly folded and faulted), locally covered by Quaternary detritic deposits.

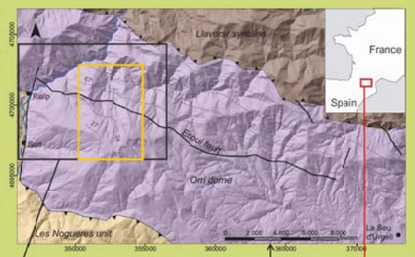

Figure 1- Geological map including the study area (yellow rectangle) adapted from (Poblet, 1991) showing the main structural units in 3 different colors, faults and thrusts (black lines), foliation traces (grey lines) and corresponding dip values.

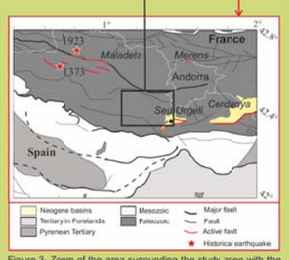

Figure 2- Geomorphological context of the study area with the main geomorphological features, rivers and main streams (orthophoto 25cm from the ICGC used as background).

Figure 3- Zoom of the area surrounding the study zone with the closest active faults, taken from Lacan and Ortuño (2012), and the location of the epicenters of the Vielha 1923 (ML 5.2, Susagna et al.,1994)) and the Ribagorçana 1373 (M= 6.2, (Olivera et al., 2006)) earthquakes.

3- LiDAR data

The lidar DEM is part of LidarCat DEM that covers Catalonia (NE Spain). Data acquisition and processing were carried out by ICGC.

In this steep area the flying height and other system parameters were set differently for each strip depending on the range of terrain elevations to be covered. Some strips had to be flown at two different flying heights to cover both the valleys and the peaks.

Bare-earth DEMs production

Lidar strips were adjusted with ground control. Points were classified into ground and vegetation and edited by trained operators and a bare earth DEM with 2 m grid step was generated. All the processing was done with Terrasolid software (TMatch, TScan & Tmodel).

Date	July-August 2009 and August-September 2011
# strips + cross strips	35 + 2
Flying speed (knots)	100-165
Flying altitude (m a.g.l.)	2113-2440
Laser repetition rate (Hz)	84400-96100
Scan frequency (Hz)	21.5-32
Scan width (FOV)	37°-48°
Swath width (m)	1620-2098
Footprint size (m)	0.48-0.59
Point density (points/m^2)	0.8-2.86
Vertical precision (cm)	11-14
Horizontal precision (cm)	28-32

Table 1- Range of flight and system parameters

4- Geomorphological analysis of the slope failures

LiDAR derived maps

- 2m hillshace maps with 45° sun height and varying azimuths at 45, 135, 225 and 315°
- Topographic map with 2 m contour interval.

Detection and mapping of large scale landslides on 2D shaded relief and contour maps

Near 120 scarps were interpreted (according to Hungr et al., 2014) as resulting from slow gravitational deformation, incipient slow flow affecting a colluvium, rotational rock-sliding and slope creep.

Four synthetic cross sections were done:

1) by extracting the XYZ coordinates (3D line) of the trace of the head scarps once projected onto the 2 m DEM
2) by using the ArcGIS spatial analyst tool which applies the "natural neighbour interpolation" to obtain the surface containing this 3D line points.

Zone C1

Head scarps length: 80-1043 m

Maximum scarps height 4 m

Average scarps height 2.5-3 m

Wideness of the close depresion defined for the double ridge: 37 m

Interpretation: Complex movement defined by i) a deformation of the colluvium dominated by an incipient slow flow in C1a and ii) rock flexural topples or extensional fractures in C1b.

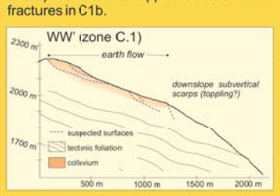

Zone C2

Scarps length: 30 m to 273 m

Scarps height: 0.5 m to 5 m

Interpretation: a combination of extensional failures and toppling and slope creep.

Zone B3

Scarps facing down-slope 60-223 m-long

Maximum height ~25 m

Opening space in double ridges: 5-6 m.

Interpretation: Northernmost scarps produced by topples and southernmost scarps produced by ridge-top spreading.

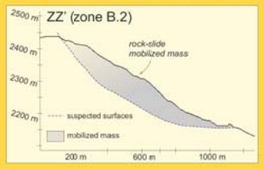

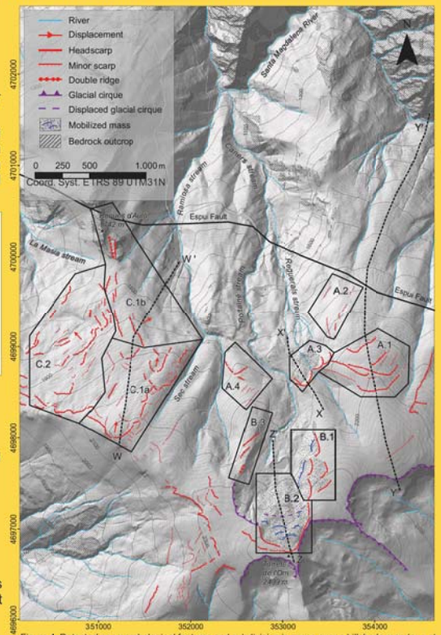

Figure 4- Detected geomorphological features and subdivision in zones over a hillshade map (sun at 45° elevation and 315° azimuth). Dotted lines correspond to the represented cross sections (smaller figures around this one).

Zones B1 and B2

Area involved: 0.32 km^2 (B2) and 0.18 km^2 (B1)

Main scarp (B2): 14 m-height and 900 m-long

Rear scarps in B1 are 5-6 m-high and 86 - 280 m-long

Interpretation: Main rotational rock-slide on the Portainé headwater (B2) and multiple smaller rotational rock-slides towards the north (B1).

Zones A1 and A2

Scarp lengths range between ~ 1 km and 100 m.

Maximum scarp height ~ 20 m

Average scarp height between 2 and 4 m

Interpretation: Major sackung with the head scarps in zone A1 and the middle slope counter scarps in zone A2

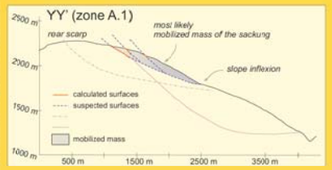

Zone A3

Composite scarp ~ 600 m long

Màximun cumulated offset 25 m at the center of the traces

Offsets along most of the scarps < 10 m

Total area apparently mobilized 0.66 km^2

Interpretation: rotational rock-slide

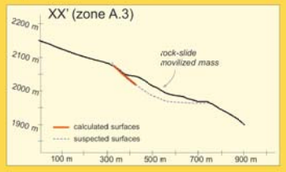

Zone A4

Uppermost scarp 223 m-long 1-2 m-high

Màximun cumulated offset 25 m at the center of the traces

Offsets along most of the scarps < 10 m

Total area apparently mobilized 0.66 km^2

Interpretation: rotational rock-slide

Analysis on 3D views

The observation of the landscape from multiple perspectives with the 3D hillshade views is useful to detect many landscape features poorly represented in the planar visualization of the hillshade maps.

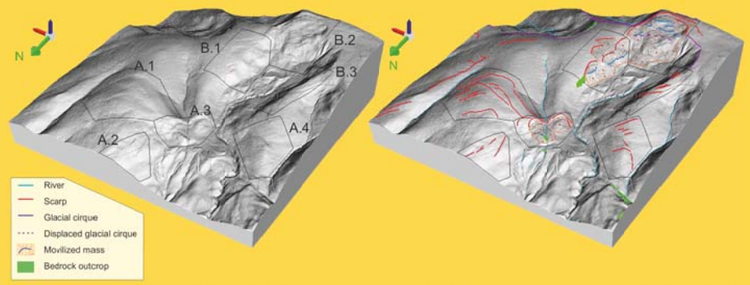

Figure 5- 3D view of the hillshade (sun azimuth 315° and sun altitude 45°) on a portion of the studied zone in the left image with the boundaries of the zones A and B, and in the right image with the geomorphological interpretation.

LiDAR DEM versus conventional methods

Geomophological interpretation of LiDAR DEM of 2 m grid step (2D and 3D views) was compared to photogrammetric DEM of 5 m grid step, ortophotos from 2010 (1:5,000) and aerial stereopairs (not presented here) from 1956 (1:26,000) and 1982 (1:30,000), where only the main landforms can be identified.

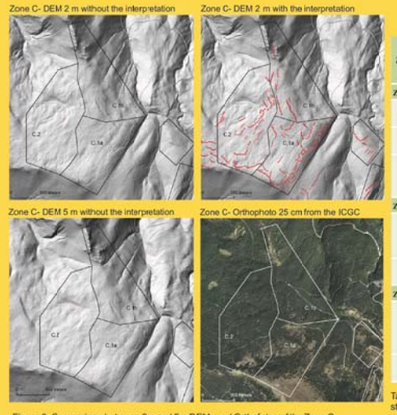

Figure 6- Comparison between 2m and 5m DEMs and Orthofotos of the Zone C

Zone (name)	Type	Length (L) and height (H) of the scarps (min - max)	Slope Dip (°)	Visible in the Aerial photos Orthophotos (Y, yes/N, not)	Visible in the 5-m topography (Y, yes/N, not)
Zone A					
A.1 +A.2	*Sackung*	L (100 - 1000 m) H (2 - 20 m)	<10 (A.1) 10-17 (A.2)	N (only major head-scarp in A.1)	N
A.3	*Rotational Rockslide*	L (312 m) H (10 - 25 m)	22 - 26	N	Y
A.4	*Sackung*	L (60 - 300 m) H (0.5 - 3.5 m)	12 - 18 (upper) ~20 (lower)	Y (in the orthophoto and non-forested area)	N
Zone B					
B.1 + B.2	*Rotational Rockslide*	L (86 - 900 m) H (5 - 14 m)		Y (although minor rear-scarps in zone B.2 are not detected)	Y
B.3		L (60 - 223 m) H (5 - 25 m)		Y	Y
Zone C					
C.1	*Colluvium Slow flow (C1.a)+ slow gravitational scarps (C1.b)*	L (80 - 1043 m) H (2.5 - 4 m)	10 - 15 (C1.a)	N (only main head scarp in zoneC1.a and double ridge in zone C1.b)	N
C.2	*Slope creep*	L(30 - 280 m) H (0.5 - 5 m)	15 - 25	N	N

Table2- Identified landslides and their delectability in the orthophoto and in the 5-m grid step DEM. In case of almost constant slope failures, the maximum slope dip is given.

5- Discussion and conclusions

The LiDAR data analysis is implemented for the first time in an area where only one large landslide had been previously detected by Hartevelt (1969, 1970).

LiDAR has proved high potential to detect incipient large-scale landslides not detectable by conventional mapping methods. LiDAR derived bare-earth topography allows to map and analyse scarps of small dimensions (under 2 m-high) located in forest areas.

The presence of vegetation and the steep terrain are limiting factors reducing the precision of LiDAR derived datasets in mountain areas that can be overcome by specific data collection flights and by trained operators processing the data.

Expert-based analysis is required to identify subtle landforms associated to incipient landslides, but introduces a subjective interpretation.

Thus, the analysis of the scarp assemblage, their location with respect to the slope and other characteristics such as the slope angle, the slope profile and the 3D appearance of the relief, led us to classify the landslides as large-scale failures: sackungs, rotational rock-slides and colluvium deformations.

The systematic analysis of LIDAR data on entire regions performed by trained geomorphologists should reveal the presence of many areas affected by landslides that otherwise would remain unknown.

References

- Hartevelt, J.J.A., 1969. Geological Map of Central Pyrenees. Sheet 10. Esc. 1:50.000.

- Hartevelt, J.J.A., 1970. Geology of the Upper Segre and Valira Valleys, Central Pyrenees, Andorra, Spain. Leidse Geol. Meded. 45, 167–236.

- Hungr, O., Leroueil, S., Picarelli, L., 2014. The Varnes classification of landslide types, an update. Landslides 11, 167–194.

- Lacan, P., Ortuño, M., 2012. Active Tectonics of the Pyrenees: 923 A review. J. Iber. Geol. 38, 9–30.

- Olivera, C., Redondo, E., Lambert, J., Riera Melis, A., Roca, A., 2006. Els terratrèmols dels segleS XIV i XV a Catalunya, Monografie. ed. Institut Cartogràfic de Catalunya, Barcelona.

- Poblet, J., 1991. Estructura herciniana i alpina del vessant sud de la zona axial del Pirineu central. Universitat de Barcelona.

- Susagna, T., Roca, A., Goula1, X., Batllo, J., 1994. Analysis of macroseismic and instrumental data for the study of the 19 November 1923 earthquake in the Aran Valley (Central Pyrenees). Nat. Hazards 10, 7–17.

- Terrasolid, 2015. Terrasolid [WWW Document]. URL http://www.terrasolid.com

Acknowledgements

This work was supported by the AGAUR 2009-SGR-520 funding of RISKNAT group, the CHARMA Spanish Project (MINECO, Ref.: CGL2013-40828-R) and the funds of the Institut Cartogràfic i Geològic de Catalunya (ICGC) for the acquisition and processing of LiDAR data.